Development of Hydrophobic Graphenoid Layer on Portland Cement for Non-Thermal Plasma Method.

N.G. Pereira Filho[a], E.P. Soares[a], J.C. Ferreira[a], R.F.B. de Souza[a]*, D.A.Andrede, A.O. Neto[a]

[a]Instituto de Pesquisas Energéticas e Nucleares, IPEN/CNEN-SP, Av. Prof. Lineu Prestes, 2242 Cidade Universitária, CEP 05508-000, São Paulo, SP, Brazil

* e-mail: souza.rfb@gmail.com

Abstract

This study focuses on the development of hydrophobic layer on Portland cement using graphenoid materials to enhance impermeability and hydrophobicity. X-ray diffraction analysis revealed that characteristic peaks associated with concrete remained intact, indicating the presence of phases such as ettringite, calcium hydroxide, calcite, and more. Remarkably, the application of graphenoid material produced by non-thermal plasma resulted in the formation of carbonaceous structures with minimal impact on the overall cement structure. Raman spectroscopy provided detailed insights into the composition, highlighting the presence of specific and indicating boundary defects. Moreover, contact angle measurements confirmed a substantial increase in hydrophobicity for the graphene-coated cement, with an average angle of 117° +/- 4.72° demonstrated graphenoid material layers deposited over structural defects, effectively waterproofing and enhancing local hydrophobicity.

Keywords; Hydrophobic covered, Graphenoid Material, Portland Cement, Non-Thermal Plasma, Impermeability Enhancement

Preprint not peer reviewed

This preprint research paper has not been peer reviewed. Electronic copy available at: https://ssrn.com/abstract=4766377

Introduction

Concrete is universally acclaimed as one of the most versatile, durable, and robust construction materials in the world. While permeability is desirable for concrete in paving applications, facilitating water drainage [1], water infiltration into concrete used for structural purposes can lead to structural decay and aesthetic concerns, ultimately diminishing the longevity of concrete structures [2, 3]. This infiltration not only jeopardizes the structural integrity of concrete but also gives rise to issues such as reinforcement corrosion and premature degradation.

In response to these challenges, there has been a burgeoning interest in developing additives that enhance the waterproofing characteristics of concrete, with the goal of extending the service life of concrete elements while simultaneously reducing the costs associated with repairs and maintenance [3, 4]. Among various techniques, surface coatings have emerged as the predominant method adopted by a majority of researchers, often evaluated through water absorption tests. This research trend highlights a notable emphasis on the utilization of polymer-based materials, silicate-containing compounds, silanes, siloxanes, cementitious materials, and specific nanomaterials. As a result, additives can be classified into three categories based on their material composition, application methodology, and functional attributes [5, 6].

Graphene, renowned for its water-repellent properties and its ability to enhance impermeability [7-9], represents a promising solution to the evolving demands of modern civil construction. It offers the potential for developing cost-effective graphene material layers capable of efficiently repelling water. Nevertheless, it is important to note that graphene remains a relatively expensive material, often applied as an additive to polymer coatings [10, 11]. However, the development of low-cost graphene production technologies has significantly bolstered the attractiveness and feasibility of incorporating graphene in construction applications.

In plasma-based methodologies [12, 13], small graphene flakes comprising only a few layers can be synthesized without the need for substrates, utilizing a rapid and precisely controlled synthesis process. Plasma synthesis entails the decomposition of a carbon source, leading to the formation of carbon particle fragments within the gaseous phase of the plasma stream.

Recently, Neto et al.'s research group [14-16] introduced a clean, rapid, and cost-effective methodology for growing graphene nanoparticles on non-conductive materials

Preprint not peer reviewed

This preprint research paper has not been peer reviewed. Electronic copy available at: https://ssrn.com/abstract=4766377

such as hexagonal boron nitride and fiberglass. This innovative approach involves the conversion of hydrocarbons into graphene-like materials using a cold plasma generator. Significantly, this method enables the direct growth of graphene onto substrates without the need for additional adhesion-promoting substances. In light of these advancements, this study proposes the utilization of a bottom-up graphene formation method on Portland cement substrates as a means to enhance the material's waterproofing capabilities.

Experimental

The cement utilized was Type I Portland cement, and the paste with a water-to-cement (w/c) ratio of 0.5 was thoroughly mixed and subsequently transferred to sample holders measuring approximately 20 mm x 20 mm x 5 mm. After hardening, the samples were demoulded and cured at room temperature after 24 hours.

The deposition of graphene onto Portland cement sample was achieved using a non-thermal plasma generator coupled to a reaction vessel, following the approach detailed in prior studies [14-16]. Within this reactor, employing cyclohexane (Aldrich) as the initial input material, a 60 kV electric arc was initiated with a flow of $N_{2(g)}$ between a 316L steel electrode and another composed of 316L steel wire, where the Portland cement sample was affixed, until complete evaporation of the liquid was observed.

The resulting dry material was then subjected to characterization through scanning electron microscopy (SEM) utilizing a Jeol JSM-6701F instrument. The block was cut transversely on an Isomet 900 cutter using a diamond blade for ceramic materials with a cutting speed of 100 rpm, without cooling. This low speed maintains the integrity of the graphene deposit in the block. X-ray diffraction (XRD) patterns were acquired using a Miniflex II diffractometer equipped with a Cu Kα radiation source (0.15406 Å wavelengths) over a 2θ range of 2–90° at a scan speed of 2 min^{-1}. Raman spectra were recorded employing a Horiba Scientific MacroRam Raman spectroscopy apparatus equipped with a 785 nm laser.

Contact angle measurements were conducted in accordance with ISO (International Organization for Standardization) methodology 15989/2004, utilizing a goniometer (KINO-SL150E) as described in the International System of Units (SI) file.

Preprint not peer reviewed

This preprint research paper has not been peer reviewed. Electronic copy available at: https://ssrn.com/abstract=4766377

For contact angle determination, 2.0 μL deionized water droplets were dispensed onto the sample surfaces. Multiple measurements were taken on a minimum of five distinct samples for each substrate, with ten readings per sample, and the average values were recorded.

Results and Discussion

In Figures 1a and 1b, cross-sectional views of hardened Portland cement and the same cement, which was covered with graphenoid material obtained through non-thermal plasma treatment, are presented. For the sample treated with carbonaceous material, a darker region is evident, indicating penetration of up to approximately 70 μm. When was switch to secondary electron imaging to examine the same region, we observe structural alterations on the material's surface, extending to around 120 to 150 μm. This altered region exhibits a softer texture compared to the bulk material, as depicted in Figure 1c. The soft texture becomes more evident upon closer examination, as seen in Figures 1d, e, and 1f. These structural modifications can be attributed to the non-thermal plasma process, which has previously demonstrated its effectiveness in altering stable structures such as SiO_2 and h-BN [15, 16].

Preprint not peer reviewed

This preprint research paper has not been peer reviewed. Electronic copy available at: https://ssrn.com/abstract=4766377

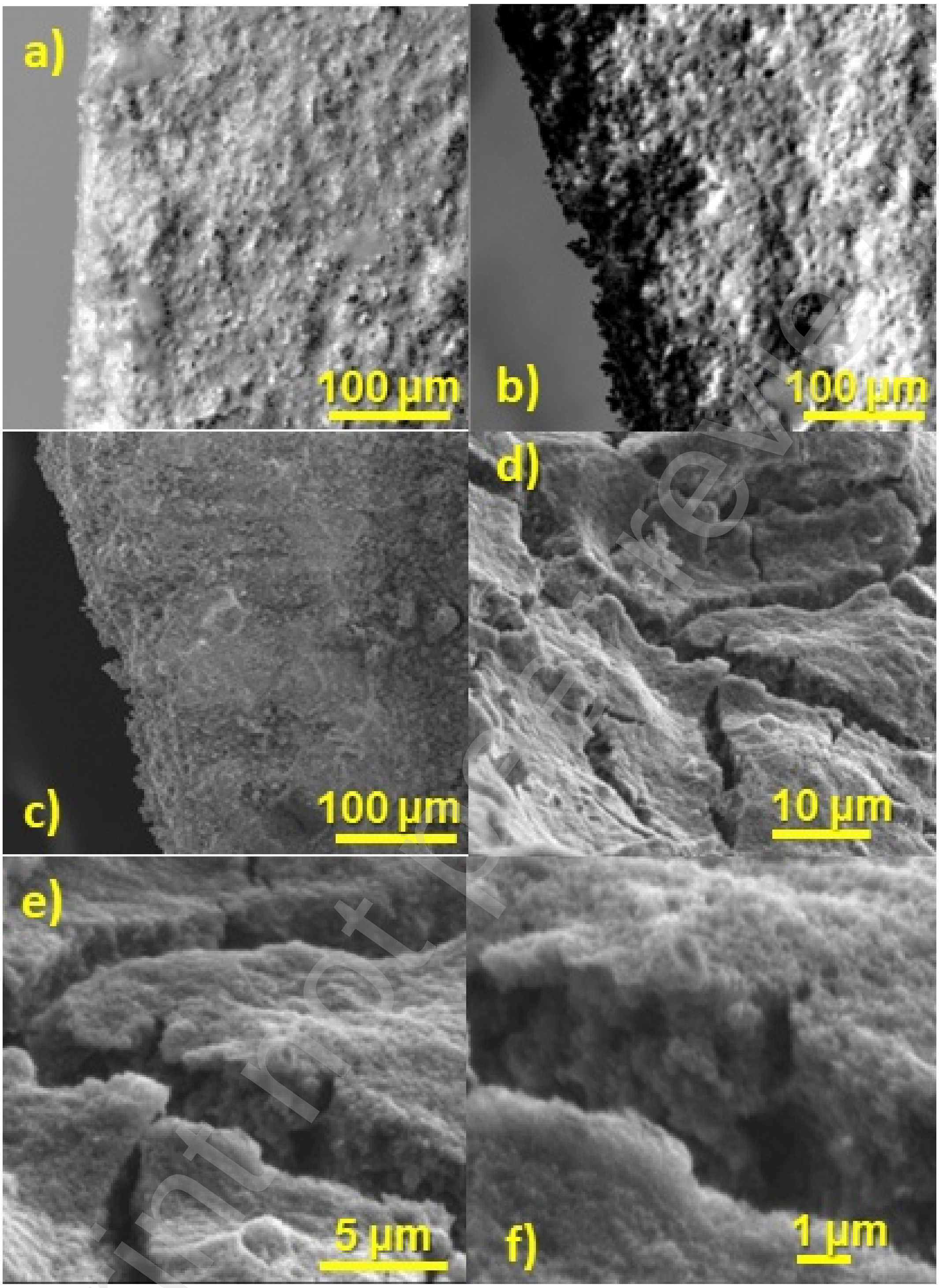

Figure 1: SEM images of a) Portland Cement, b) Covered Portland Cement, c) SEI of Covered Portland Cement with a magnification of 250x, d) 2000x, e) 5000x, and f) 10000x.

Fig. 2 shows XRD patterns of the PC with and without graphenoid layer, and is possible to observe all characteristic peaks of the Portland cement, these peaks are related to the presence of ettringite at around 2θ ~ 23º, 31º, and 33º, resulting from the sulphate ion's reaction with calcium-bearing compounds. Calcite, with its characteristic

Preprint not peer reviewed

This preprint research paper has not been peer reviewed. Electronic copy available at: https://ssrn.com/abstract=4766377

peak at ~26º, is the primary hydration product in cement composites and is also present in gypsum compounds [17]. Other notable peaks include portlandite at 48º [18], quartz around ~38º and 52º [19], alite at ~ 29º, 32º, and 62º degrees, convoluted at ~30º and 33º from belite, and calcium hydroxide at ~18º, 34º, and 47º degrees [20]. In the absence of peak shifts, these results suggest that the structure was largely unaffected by the non-thermal plasma treatment, except for the absence of the 18° peak in the coated sample.

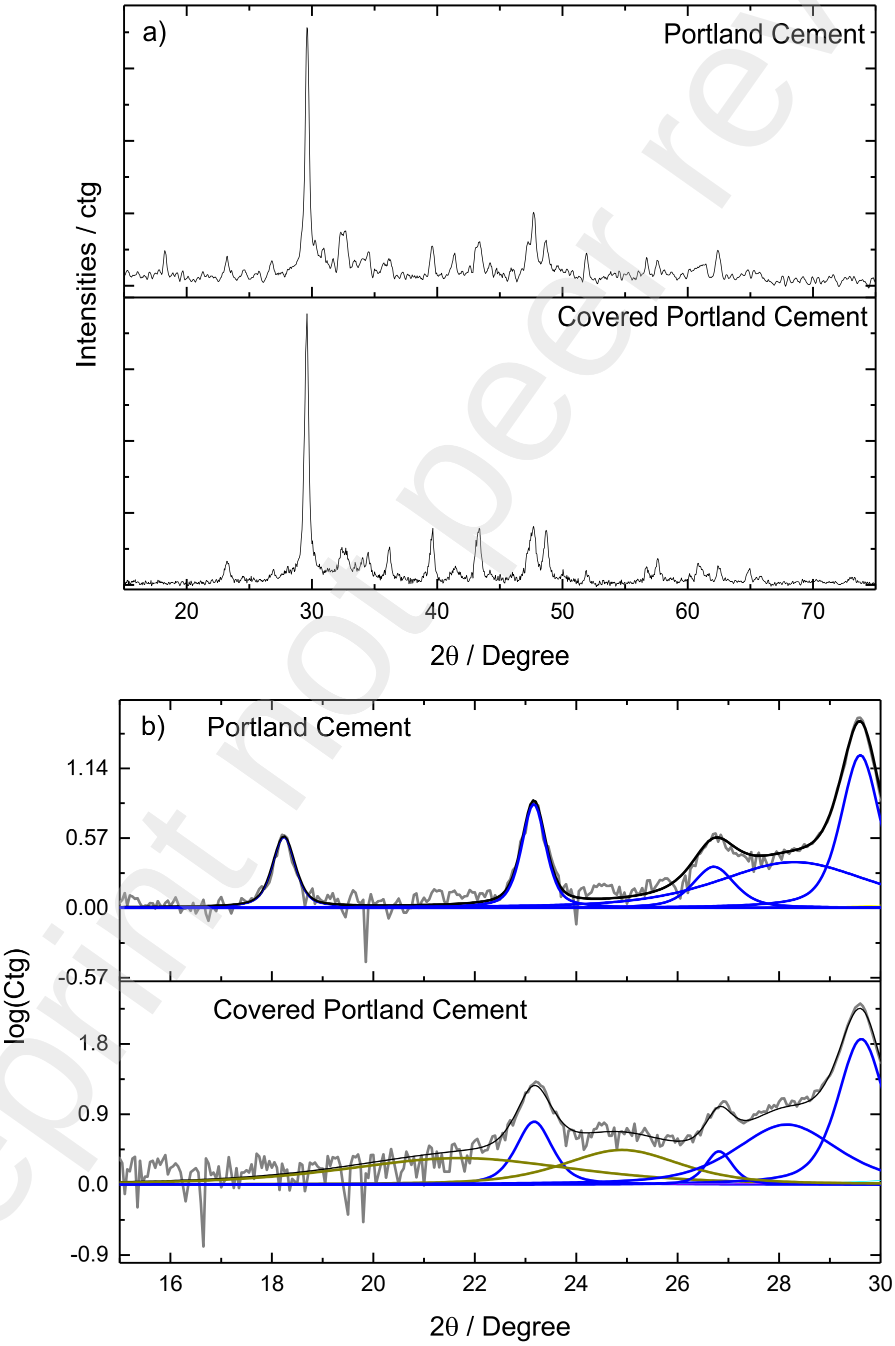

Preprint not peer reviewed

This preprint research paper has not been peer reviewed. Electronic copy available at: https://ssrn.com/abstract=4766377

Figure 2: a) X-ray diffraction patterns of Portland Cement and Covered Portland Cement. b) Logarithm of the intensities obtained from the X-ray diffraction patterns measured for Portland Cement, with deconvolution of the peak corresponding to the (002) plane, as well as carbon diffraction.

Additionally, the method of depositing graphenoid nanoflakes via non-thermal plasma on cement results in the formation of carbonaceous structures with a few layers [14, 15], which can render carbon phases not directly observable through X-ray diffraction for certain materials, primarily due to differences in crystallite size. As depicted in Figure 2b, the XRD pattern was plotted on a logarithmic scale to investigate the potential presence of graphene within the concrete sample. Examination of the graphene's crystallographic pattern reveals indications of nanoflakes stacking and crystalline dimensions within the graphene crystal lattice. These distinctive characteristics manifest in the (002) and (100) planes, which display diffraction peaks approximately at $2\theta \sim 22.3°$ and 24.9°[14], respectively, in conjunction with the diffraction peaks corresponding to the cement phases.

Utilizing Raman spectroscopy (Figure 3), an array of distinct spectral bands within Portland Cement was discerned. Specifically, prominent bands corresponding to ettringite at 1160 cm^{-1}[21], and a noteworthy band at 1440 cm^{-1}, associated with ettringite $Ca_6Al_2O_6(SO_{4)}.14H_2O$ and linked to the sulphate $\nu_2SO_4^{2-}$ mode [22]. Furthermore, the spectral analysis revealed discernible bands at 1485 cm^{-1} and 1765 cm^{-1}, denoting the presence of calcium hydroxide [23], and a band at 1249 cm^{-1}, correlated with $Ca.H_2O_5Si^{2-}$[24]. Noteworthy contributions also included a distinctive signature at 1624 cm^{-1} for calcium oxide [25], a discernible peak at 1680 cm^{-1} attributable to $3CaO.Al_2O_3$[26], and a band at 1085 cm^{-1}[27]. The latter was ascribed to calcite (1070 cm^{-1}) [28], while alternatively, the peak at 1081 cm^{-1} was associated with the symmetrical stretching mode of Si-O tetrahedra [29], it is imperative to underscore that these proposed identifications are not mutually exclusive; rather, the observed spectrum may encompass a combination thereof.

Preprint not peer reviewed

This preprint research paper has not been peer reviewed. Electronic copy available at: https://ssrn.com/abstract=4766377

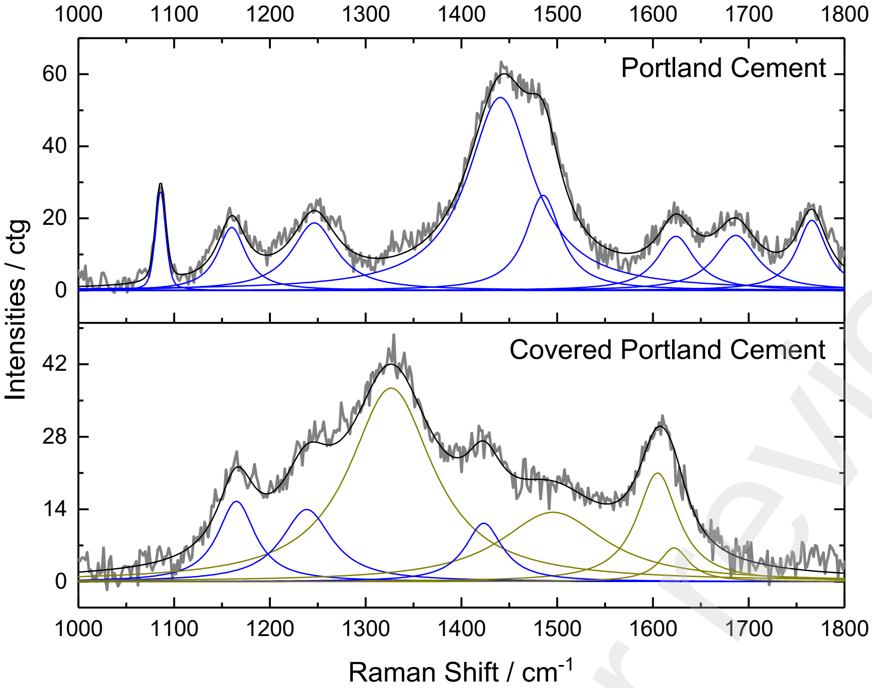

Figure 3: Raman Spectrum of the Portland Cement and Covered Porland Cement deconvolved in range of 1000 and 1800 cm^{-1}. In blue the cement bands and in dark yellow the carbon bands.

Upon scrutinizing the Covered Portland Cement sample, a conspicuous suppression of the majority of bands associated with Portland Cement became evident. Instead, distinctive peaks corresponding to the D1, D2, D3, and G modes of carbon at approximately 1322, 1623, 1495, and 1587 cm^{-1}, respectively, were observed [30]. These outcomes provide clear evidence of a partial coverage overlaying the Portland Cement substrate.

The literature extensively discusses the G-band, which corresponds to the first-order scattering of the E_{2g} mode associated with sp^2 carbon. Additionally, the D band can be attributed to structural defects, carbon amorphism, or edge defects, all of which have the potential to disrupt symmetry and selection rules [31]. The G band's characteristics are influenced by the number of layers, reflecting the contribution of the vibrational mode involving more carbon atoms. Changes in its intensity, shape, and position serve as indicators of induced deformations. Notably, within the literature, the Raman intensity ratio of the D-band to G-band (I_D/I_G) stands as a pivotal parameter for assessing the degree of disorder in graphene [32]. In the case of this sample, the obtained value of 3.5 signifies the presence of boundary defects.

Preprint not peer reviewed

This preprint research paper has not been peer reviewed. Electronic copy available at: https://ssrn.com/abstract=4766377

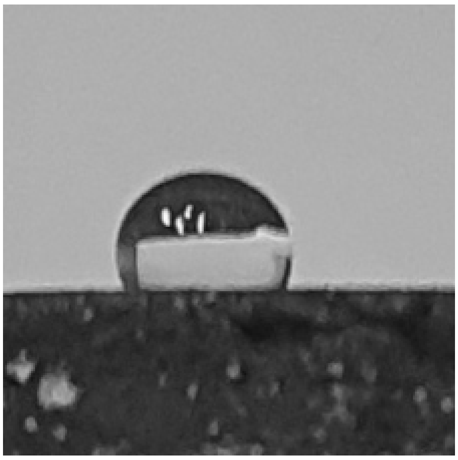

Figure 4. Contact angle result image of Covered Portland Cement.

The hydrophobicity was assessed through contact angle measurements (Figure 4), yielding an average angle of 117° +/- 4.72°, in stark contrast to the behavior observed in plain Portland cement, where water droplets are readily absorbed. This result is in agrément with the observed in figure 1, where we observe layers of graphenoid materials deposited on the defects of the cement structure, rendering it impermeable and increasing local hydrophobicity. The application of graphene to the Portland cement surface has brought about a remarkable shift in wettability characteristics. This substantial increase in the contact angle, indicative of enhanced hydrophobicity due to graphene application, underscores the beneficial impact of the coating on the cement surface. Such a modification in wettability properties carries significant implications for bolstering water infiltration resistance and augmenting the durability of concrete structures.

Conclusion

The non-thermal plasma applied to convert cyclohexane into a graphene hydrophobic layer on Portland Cement was very promising. The X-ray diffraction analysis revealed that the characteristic peaks of concrete remained evident, indicating the presence of ettringite and other phases typically associated with Portland Cement. The absence of peak shifts suggested that the overall structure was minimally affected by the non-thermal plasma treatment. Moreover, the formation of graphenoid film via non-thermal plasma resulted in the formation of carbonaceous structures with a few layers block on the Portland Cement. The Raman spectroscopy provided valuable insights into the concrete's composition, with distinct spectral bands indicating the

Preprint not peer reviewed

This preprint research paper has not been peer reviewed. Electronic copy available at: https://ssrn.com/abstract=4766377

presence of ettringite, calcium hydroxide, calcite, and other phases. Notably, the Raman intensity ratio of the D-band to G-band (ID/IG) yielded a value of 3.5 for this sample, indicative of boundary defects. Additionally, the water contact angle measurements confirmed a significant increase in hydrophobicity, with an average angle of 117° +/- 4.72° observed for the graphene-coated cement, in contrast to the immediate absorption of water droplets by plain Portland cement. In summary, the application of graphenoid materials to cement surfaces has demonstrated the potential to transform its properties, offering improved water resistance and hydrophobicity. These findings hold promise for enhancing the durability and longevity of concrete structures, particularly in scenarios where water infiltration poses a significant challenge.

Acknowledgment

We are grateful to CAPES, CNPq (350514/2023-2, 302709/2020-7), COPDE/IPEN (2020.06.IPEN.05), for financial supports.

References

[1] N. Xie, M. Akin, X. Shi, Permeable concrete pavements: A review of environmental benefits and durability, Journal of Cleaner Production, 210 (2019) 1605-1621. https://doi.org/10.1016/j.jclepro.2018.11.134

[2] X. Xiao, J. Li, D. Cai, H. Cheng, F. Xiao, Characterizing thermal fatigue behaviors of asphalt concrete waterproofing layer in high-speed railway using customized overlay test, International Journal of Fatigue, 165 (2022) 107176. https://doi.org/10.1016/j.ijfatigue.2022.107176

[3] N.Z. Muhammad, A. Keyvanfar, M.Z. Abd. Majid, A. Shafaghat, J. Mirza, Waterproof performance of concrete: A critical review on implemented approaches, Construction and Building Materials, 101 (2015) 80-90. https://doi.org/10.1016/j.conbuildmat.2015.10.048

[4] A. Garbacz, M. Górka, L. Courard, Effect of concrete surface treatment on adhesion in repair systems, Magazine of Concrete Research, 57 (2005) 49-60. 10.1680/macr.2005.57.1.49

[5] P.A.M. Basheer, L. Basheer, D.J. Cleland, A.E. Long, Surface treatments for concrete: assessmentmethods and reported performance, Construction and Building Materials, 11 (1997) 413-429. https://doi.org/10.1016/S0950-0618(97)00019-6

[6] M. Horgnies, P. Willieme, O. Gabet, Influence of the surface properties of concrete on the adhesion of coating: Characterization of the interface by peel test and FT-IR spectroscopy, Progress in Organic Coatings, 72 (2011) 360-379. https://doi.org/10.1016/j.porgcoat.2011.05.009

[7] O. Leenaerts, B. Partoens, F.M. Peeters, Water on graphene: Hydrophobicity and dipole moment using density functional theory, Physical Review B, 79 (2009) 235440. 10.1103/PhysRevB.79.235440

[8] Z. Zhou, S. Li, J. Cao, X. Chen, Z. Wu, P. Zhou, The waterproofing effect and mechanism of graphene oxide/silane composite emulsion on cement-based materials

Preprint not peer reviewed

This preprint research paper has not been peer reviewed. Electronic copy available at: https://ssrn.com/abstract=4766377

under compressive stress, Construction and Building Materials, 308 (2021) 124945. https://doi.org/10.1016/j.conbuildmat.2021.124945

[9] Q.G. Jiang, Z.M. Ao, D.W. Chu, Q. Jiang, Reversible Transition of Graphene from Hydrophobic to Hydrophilic in the Presence of an Electric Field, The Journal of Physical Chemistry C, 116 (2012) 19321-19326. 10.1021/jp3050466

[10] Y. Zhang, S. Li, W. Zhang, X. Chen, D. Hou, T. Zhao, X. Li, Preparation and mechanism of graphene oxide/isobutyltriethoxysilane composite emulsion and its effects on waterproof performance of concrete, Construction and Building Materials, 208 (2019) 343-349. https://doi.org/10.1016/j.conbuildmat.2019.03.015

[11] X. Chen, Y. Zhang, S. Li, Y. Geng, D. Hou, Influence of a New Type of Graphene Oxide/Silane Composite Emulsion on the Permeability Resistance of Damaged Concrete, Coatings, 2021. 10.3390/coatings11020208

[12] A. Dato, Graphene synthesized in atmospheric plasmas—A review, Journal of Materials Research, 34 (2019) 214-230. 10.1557/jmr.2018.470

[13] M.B. Shavelkina, E.A. Filimonova, R.K. Amirov, Effect of helium/propane–butane atmosphere on the synthesis of graphene in plasma jet system, Plasma Sources Science and Technology, 29 (2020) 025024. 10.1088/1361-6595/ab61e3

[14] P.V.R. Gomes, N.F.B. Azeredo, L.M.S. Garcia, P.J. Zambiazi, G.R. Morselli, R.A. Ando, L. Otubo, D.R.R. Lazar, R.F.B. de Souza, D.F. Rodrigues, A.O. Neto, Layered graphene/hexagonal boron nitride nanosheets (Gr/h-BNNs) applied to the CO2 photoconversion into methanol, Applied Materials Today, 29 (2022) 101605. https://doi.org/10.1016/j.apmt.2022.101605

[15] P.V.R. Gomes, R.N. Bonifacio, B.P.G. Silva, J.C. Ferreira, R.F.B. de Souza, L. Otubo, D.R.R. Lazar, A.O. Neto, Graphene Deposited on Glass Fiber Using a Non-Thermal Plasma System, Eng, 2023, pp. 2100-2109. 10.3390/eng4030119

[16] R.F.B. de Souza, V.A. Maia, P.J. Zambiazzi, L. Otubo, D.R.R. Lazar, A.O. Neto, Facile, clean and rapid exfoliation of boron-nitride using a non-thermal plasma process, Materials Today Advances, 12 (2021) 100181. https://doi.org/10.1016/j.mtadv.2021.100181

[17] K. Chintalapudi, R.M.R. Pannem, Enhanced chemical resistance to sulphuric acid attack by reinforcing Graphene Oxide in Ordinary and Portland Pozzolana cement mortars, Case Studies in Construction Materials, 17 (2022) e01452. https://doi.org/10.1016/j.cscm.2022.e01452

[18] V.D. Ho, C.-T. Ng, T. Ozbakkaloglu, A. Goodwin, C. McGuckin, R.U. Karunagaran, D. Losic, Influence of pristine graphene particle sizes on physicochemical, microstructural and mechanical properties of Portland cement mortars, Construction and Building Materials, 264 (2020) 120188. https://doi.org/10.1016/j.conbuildmat.2020.120188

[19] S. Du, Z. Tang, J. Zhong, Y. Ge, X. Shi, Effect of admixing graphene oxide on abrasion resistance of ordinary portland cement concrete, AIP Advances, 9 (2019). 10.1063/1.5124388

[20] V.D. Ho, C.-T. Ng, C.J. Coghlan, A. Goodwin, C. Mc Guckin, T. Ozbakkaloglu, D. Losic, Electrochemically produced graphene with ultra large particles enhances mechanical properties of Portland cement mortar, Construction and Building Materials, 234 (2020) 117403. https://doi.org/10.1016/j.conbuildmat.2019.117403

[21] J. Bensted, Uses of Raman Spectroscopy in Cement Chemistry, Journal of the American Ceramic Society, 59 (1976) 140-143. https://doi.org/10.1111/j.1151-2916.1976.tb09451.x

[22] R. Masmoudi, K. Kupwade-Patil, A. Bumajdad, O. Büyüköztürk, In situ Raman studies on cement paste prepared with natural pozzolanic volcanic ash and Ordinary

Preprint not peer reviewed

This preprint research paper has not been peer reviewed. Electronic copy available at: https://ssrn.com/abstract=4766377

Portland Cement, Construction and Building Materials, 148 (2017) 444-454. https://doi.org/10.1016/j.conbuildmat.2017.05.016

[23] F. Liu, Z. Sun, C. Qi, Raman Spectroscopy Study on the Hydration Behaviors of Portland Cement Pastes during Setting, Journal of Materials in Civil Engineering, 27 (2015) 04014223. 10.1061/(ASCE)MT.1943-5533.0001189

[24] M. Azeem, M.A. Saleem, A Raman Spectroscopic Study of Calcium Silicate Hydrate (CSH) in the Cement Matrix with CNTs and Oxide Additives, Journal of Spectroscopy, 2022 (2022) 2281477. 10.1155/2022/2281477

[25] G. Ovcharenko, E. Ibe, A.J.E.S.W.C. Viktorov, Assessment of the influence of additives in concrete by the Raman spectroscopy method, 157 (2020) 06004.

[26] J.J. Soto-Bernal, R. Gonzalez-Mota, I. Rosales-Candelas, J.A. Ortiz-Lozano, Effects of Static Magnetic Fields on the Physical, Mechanical, and Microstructural Properties of Cement Pastes, Advances in Materials Science and Engineering, 2015 (2015) 934195. 10.1155/2015/934195

[27] I.G. Richardson, J. Skibsted, L. Black, R.J. Kirkpatrick, Characterisation of cement hydrate phases by TEM, NMR and Raman spectroscopy, 22 (2010) 233-248. 10.1680/adcr.2010.22.4.233

[28] N. Garg, K. Wang, S.W. Martin, A Raman spectroscopic study of the evolution of sulfates and hydroxides in cement–fly ash pastes, Cement and Concrete Research, 53 (2013) 91-103. https://doi.org/10.1016/j.cemconres.2013.06.009

[29] M. Vetter, J. Gonzalez-Rodriguez, E. Nauha, T. Kerr, The use of Raman spectroscopy to monitor phase changes in concrete following high temperature exposure, Construction and Building Materials, 204 (2019) 450-457. https://doi.org/10.1016/j.conbuildmat.2019.01.165

[30] Z. Lu, C. Wang, X. Chen, M. Song, W. Xia, Effects of buffer gas on N-doped graphene in a non-thermal plasma process, Diamond and Related Materials, 118 (2021) 108548. https://doi.org/10.1016/j.diamond.2021.108548

[31] J.-B. Wu, M.-L. Lin, X. Cong, H.-N. Liu, P.-H. Tan, Raman spectroscopy of graphene-based materials and its applications in related devices, Chemical Society Reviews, 47 (2018) 1822-1873. 10.1039/C6CS00915H

[32] A.C. Ferrari, D.M. Basko, Raman spectroscopy as a versatile tool for studying the properties of graphene, Nature Nanotechnology, 8 (2013) 235-246. 10.1038/nnano.2013.46

Preprint not peer reviewed

This preprint research paper has not been peer reviewed. Electronic copy available at: https://ssrn.com/abstract=4766377